inorganics

MDPI

Article

Investigations on the Spin States of Two Mononuclear Iron(II) Complexes Based on N-Donor Tridentate Schiff Base Ligands Derived from Pyridine-2,6-Dicarboxaldehyde

Yosef Bayeh [1,2,3], Nithin Suryadevara [4], Sören Schlittenhardt [5], Róbert Gyepes [6], Assefa Sergawie [1,2], Peter Hrobárik [3,*], Wolfgang Linert [7], Mario Ruben [4,5,8,*] and Madhu Thomas [1,2,*]

1 Department of Industrial Chemistry, College of Applied Sciences, Addis Ababa Science and Technology University, Addis Ababa P.O. Box 16417, Ethiopia; yosef.bayeh@aastu.edu.et (Y.B.); assefa.sergawie@aastu.edu.et (A.S.)
2 Nanotechnology Center of Excellence, Addis Ababa Science and Technology University, Addis Ababa P.O. Box 16417, Ethiopia
3 Department of Inorganic Chemistry, Faculty of Natural Sciences, Comenius University, Mlynská dolina CH-2, Ilkovičova 6, 84215 Bratislava, Slovakia
4 Institute of Quantum Materials and Technologies, Karlsruhe Institute of Technology, Hermann-von-Helmholtz-Platz 1, 76344 Karlsruhe, Germany; nithin.suryadevara@kit.edu
5 Institute of Nanotechnology, Karlsruhe Institute of Technology, Hermann-von-Helmholtz-Platz 1, 76344 Karlsruhe, Germany; soeren.schlittenhardt@kit.edu
6 Department of Inorganic Chemistry, Faculty of Science, Charles University in Prague, Hlavova 2030/8, 12843 Prague, Czech Republic; gyepes@natur.cuni.cz
7 Institute of Applied Physics, Vienna University of Technology, Wiedner Hauptstraße 8-10, 1040 Vienna, Austria; wolfgang.linert@tuwien.ac.at
8 Centre Européen de Science Quantique (CESQ), Institut de Science et d'Ingénierie Supramoléculaires (ISIS, UMR 7006), CNRS-Université de Strasbourg, 8 Allée Gaspard Monge, BP 70028, CEDEX, 67083 Strasbourg, France
* Correspondence: peter.hrobarik@uniba.sk (P.H.); mario.ruben@kit.edu (M.R.); madhu.thomas@aastu.edu.et (M.T.)

check for updates

Citation: Bayeh, Y.; Suryadevara, N.; Schlittenhardt, S.; Gyepes, R.; Sergawie, A.; Hrobárik, P.; Linert, W.; Ruben, M.; Thomas, M. Investigations on the Spin States of Two Mononuclear Iron(II) Complexes Based on N-Donor Tridentate Schiff Base Ligands Derived from Pyridine-2,6-Dicarboxaldehyde. *Inorganics* **2022**, *10*, 98. https://doi.org/10.3390/inorganics10070098

Academic Editor: László Kótai

Received: 31 May 2022
Accepted: 6 July 2022
Published: 8 July 2022

Publisher's Note: MDPI stays neutral with regard to jurisdictional claims in published maps and institutional affiliations.

Copyright: © 2022 by the authors. Licensee MDPI, Basel, Switzerland. This article is an open access article distributed under the terms and conditions of the Creative Commons Attribution (CC BY) license (https://creativecommons.org/licenses/by/4.0/).

Abstract: Iron(II)-Schiff base complexes are a well-studied class of spin-crossover (SCO) active species due to their ability to interconvert between a paramagnetic high spin-state (HS, S = 2, $^5T_2$) and a diamagnetic low spin-state (LS, S = 0, $^1A_1$) by external stimuli under an appropriate ligand field. We have synthesized two mononuclear Fe^{II} complexes, viz., $[Fe(L^1)_2](ClO_4)_2.CH_3OH$ (**1**) and $[Fe(L^2)_2](ClO_4)_2.2CH_3CN$ (**2**), from two N_6–coordinating tridentate Schiff bases derived from 2,6-bis[(benzylimino)methyl]pyridine. The complexes have been characterized by elemental analysis, electrospray ionization–mass spectrometry (ESI-MS), Fourier-transform infrared spectroscopy (FTIR), solution state nuclear magnetic resonance spectroscopy, ^1H and ^{13}C NMR (both theoretically and experimentally), single-crystal diffraction and magnetic susceptibility studies. The structural, spectroscopic and magnetic investigations revealed that **1** and **2** are with Fe–N_6 distorted octahedral coordination geometry and remain locked in LS state throughout the measured temperature range from 5–350 K.

Keywords: Iron(II) complexes; Schiff base; octahedral; spin-crossover and low spin

1. Introduction

Ever since the very first report on spin-crossover (SCO) compounds in early 1931 [1], numerous reports have been devoted to this spectacular field of molecular magnetism [2–4]. Among these, octahedral Fe^{II} compounds has received special attention due to the clear discrimination between the paramagnetic high spin state (S = 2, $^5T_2$) and diamagnetic low spin state (S = 0, $^1A_1$), occurring with external stimuli in an appropriate ligand field [5–8]. Intermolecular interactions, such as π-π stacking or hydrogen bonding, usually enhance the SCO behavior with abrupt transitions and hysteresis loops [9,10].

Nano-sized SCO complexes are highly relevant for considering future applications and offer diverse pathways towards multifunctional systems for molecular memory, switches or display devices [10–18]. For acquiring a desired property, it is key to tune the ligand field, which could eventually modulate the magnetic properties. It has been observed that a N_6– [19,20] or N_4O_2– [21] coordination environment around Fe^{II} can bring about sharp SCO with appreciable hysteresis width [22,23]. The effects of halogen substitution on the SCO behavior have been reported in Fe^{II}–N_6 compounds [24–30], and the spin transition temperature, $T_{1/2}$, is found to increase upon moving from fluoride to bromide substitution, thereby proving the size effect on the spin state of the complexes [20,24,31].

Previously, we have reported on how N_6–coordination and variation in the ligand field in a series of bispyrazolone derivatives brought abrupt SCO at around room temperature [32]. Additionally, in our previous reviews, the role of azomethine and substituent effects in tuning the SCO behavior and attaining the desired architecture have been inferred [8,33]. In this context, Schiff bases are ideal candidates on account of their fine tunability to the ligand field by varying the substituents in both amine and aldehydic precursors.

Recently, we have observed that N_6–coordination in Fe^{II} complexes from four azomethine and two pyridine nitrogens locks the spin state completely to a low spin condition even with an electron-donating methyl group attached to the meta position [34].

On account of the above facts and considering ligand-field and electronic effects, we are herein reporting our investigations on the structural and spin-state of two mononuclear Fe^{II} Schiff base complexes having N_6–coordination. The ligands were designed without a substituent in L^1 (2,6-bis[(benzylimino)methyl]pyridine) and with an electron-withdrawing chloro substituent at the meta position in L^2 (2,6-bis[(3–chlorobenzylimino)methyl]pyridine) in comparison with the electron-donating methyl group of the previous reports [34,35].

2. Results and Discussion

2.1. Schiff Bases L^1 and L^2 and Their Complexes **1** *and* **2**

Both ligands were prepared by condensation reaction, where benzylamine or 3-chloro benzylamine were allowed to condense with pyridine-2,6-dicarboxaldehyde in ethanol under reflux (Scheme 1). Single crystals of L^1, appropriate for X-ray diffraction studies, were grown by the slow evaporation of the solvent from a methanolic solution of L^1 at room temperature. However, we were unsuccessful in generating single crystals for L^2.

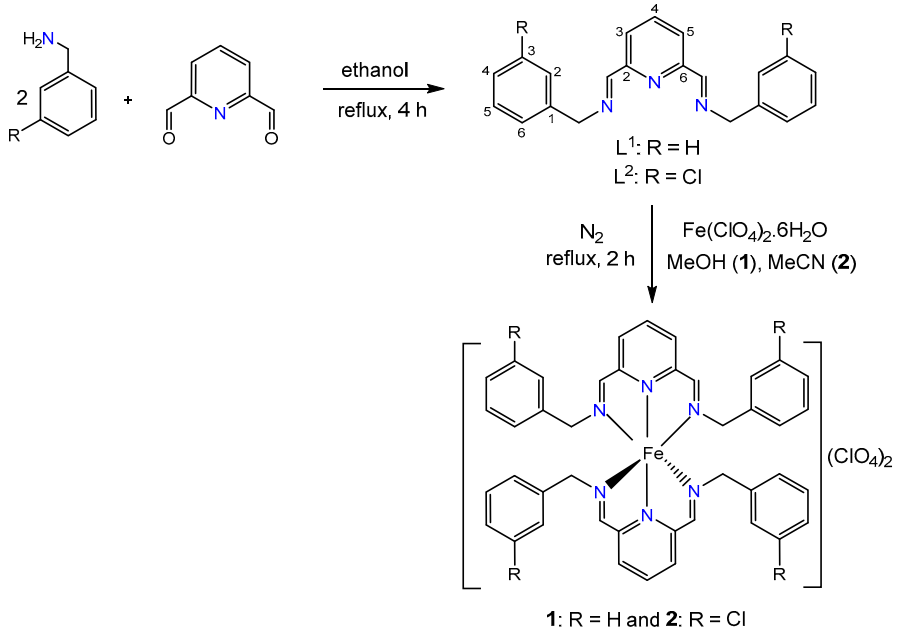

Scheme 1. Synthetic route for ligands L^1, L^2 and complexes **1** and **2**.

The corresponding complexes **1** and **2** were synthesized by the reaction of the tridentate ligands L^1 and L^2 with $Fe(ClO_4)_2 \cdot 6H_2O$ in methanol for **1** and acetonitrile for **2**, respectively (Scheme 1). Upon slow diffusion of diethylether into mother liquor at room temperature, black block crystals were obtained.

The ^1H and ^{13}C NMR spectra exhibit key resonances at 8.42 and 162.4 ppm, respectively, for L^1, and 8.43 and 163.0 ppm, respectively, for L^2, assigned to the imine (CH=N) group. The ^1H and ^{13}C NMR resonances of pyridine moiety are observed between 7.97–7.79 and 154.6–121.8 ppm, respectively, for L^1, whereas for L^2, they are between 8.00–7.81 and 154.4–122.0 ppm, respectively (see Tables 1 and 2 for more detailed assignments and Tables S1 and S2 in Supplementary Materials for DFT computed NMR chemical shifts).

Table 1. Experimental ^1H NMR shifts (in ppm vs. TMS) in free ligands L^1, L^2 and corresponding $[Fe(L^1)_2]^{2+}$ and $[Fe(L^2)_2]^{2+}$ complexes (all measured in CD_3CN) [a].

	H-Imine	**py-3,5**	**py-4**	**CH_2**	**H-2/H-6**	**H-3/H-5**	**H-4**	
L^1	8.42	7.97	7.79	4.79	7.30	7.29	7.21	
$[Fe(L^1)_2]^{2+}$	7.73	8.13	8.38	3.68	6.47	7.16	7.29	
$\Delta\delta(^1H)$ [b]	−0.69	+0.16	+0.59	−1.11	−0.83	−0.13	+0.08	
	H-Imine	**py-3,5**	**py-4**	**CH_2**	**H-2**	**H-4**	**H-5**	**H-6**
L^2	8.43	8.00	7.81	4.77	7.34	7.25	7.25	7.25
$[Fe(L^2)_2]^{2+}$	7.84	8.23	8.50	3.74	6.48	7.17	7.33	6.48
$\Delta\delta(^1H)$ [b]	−0.59	+0.23	+0.69	−1.03	−0.86	−0.08	+0.08	−0.77

[a] See SI for corresponding NMR spectra and computed chemical shifts. [b] ^1H NMR coordination shifts as a difference between resonance of given ^1H nuclei in complex and the free ligand. See Scheme 1 for atom numbering.

Table 2. Experimental ^{13}C NMR shifts (in ppm vs. TMS) in free ligands L^1, L^2 and corresponding $[Fe(L^1)_2]^{2+}$ and $[Fe(L^2)_2]^{2+}$ complexes (all measured in CD_3CN) [a].

	C-Imine	**py-2,6**	**py-3,5**	**py-4**	**CH_2**	**C-1**	**C-2/C-6**	**C-3/C-5**	**C-4**		
L^1	162.4	154.6	121.8	137.5	64.3	139.3	128.5	128.2	127.1		
$[Fe(L^1)_2]^{2+}$	170.1	160.3	128.5	137.4	62.4	133.3	128.7	129.3	129.3		
$\Delta\delta(^{13}C)$ [b]	+7.7	+5.7	+6.6	−0.1	−1.9	−6.0	+0.2	+1.2	+2.2		
	C-Imine	**py-2,6**	**py-3,5**	**py-4**	**CH_2**	**C-1**	**C-2**	**C-3**	**C-4**	**C-5**	**C-6**
L^2	163.0	154.4	122.0	133.8	63.4	141.8	128.0	137.6	127.0	130.1	126.6
$[Fe(L^2)_2]^{2+}$	171.1	160.4	128.6	135.5	61.8	134.5	128.7	137.8	130.9	129.6	127.3
$\Delta\delta(^{13}C)$ [b]	+8.1	+5.9	+6.6	+1.7	−1.6	−7.3	+0.8	+0.2	+3.9	−0.5	+0.7

[a] See SI for corresponding NMR spectra and computed chemical shifts. [b] ^{13}C NMR coordination shifts as a difference between resonance of given ^{13}C nuclei in complex and the free ligand. See Scheme 1 for atom numbering.

Upon coordination of L^1 or L^2 with Fe^{II}, the imine ^1H NMR peaks are low-frequency shifted to 7.73 ppm (**1**) and 7.84 ppm (**2**), while the imine carbons are deshielded to 170.1 ppm (**1**) and 171.1 ppm (**2**), thus by more than +7.7 ppm. Even larger ^1H shielding effects upon Fe^{II} complexation are observed for benzylic CH_2 groups ($\Delta\delta(^1H)$ = ca. −1.1 ppm) and ortho-hydrogens ($\Delta\delta(^1H)$ = ca. −0.8 ppm). Contrarily, the largest coordination-induced ^1H deshieldings ($\Delta\delta(^1H)$~+0.6 ppm) are seen for hydrogens of the pyridine moiety at the position 4 (py-4). Apart from the imine ^{13}C nuclei, the coordination-induced deshieldings are also observed for pyridine-2/-6 and pyridine-3/-5 carbons, while benzylic C-1 carbons on the phenyl ring possess the most pronounced coordination-induced shielding ($\Delta\delta(^{13}C)$ = −6 to −7 ppm).

The IR peaks were observed at 1644 cm^{-1} and 1651 cm^{-1} for L^1 and L^2, respectively, confirming the presence of CH=N. The IR spectra of L^1 and L^2 exhibit peaks at 1570 and 1594 cm^{-1}, respectively, corresponding to the pyridine C=N stretching vibration [36]. Additionally, the IR spectra of **1** and **2** show a strong band at 1603, 1528 cm^{-1} (**1**) and 1600,

1529 cm^{-1} (**2**), confirming the coordination of the azomethine and pyridine nitrogen atoms to the metal centers [37,38]. Moreover, the elemental analysis and ESI-MS measurements are also in conformity with the molecular formulae assigned, $[Fe(L^1)_2](ClO_4)_2 \cdot CH_3OH$ and $[Fe(L^2)_2](ClO_4)_2 \cdot 2CH_3CN$ for **1** and **2**, respectively.

2.2. X-ray Crystallographic Analysis

The crystallographic data of the ligand L^1 and complexes **1** and **2** are collated in Table 3; bond lengths (Table 4) and bond angles (Table S3) of **1** and **2** are also presented. For L^1, X–ray quality crystals were grown by slow evaporation of its methanolic solution. The compound crystallizes in a triclinic lattice and space group $P\bar{1}$ with two symmetrically independent molecules located in the asymmetric part of the unit cell ($Z = 4$). The crystal structure is shown in Figure 1.

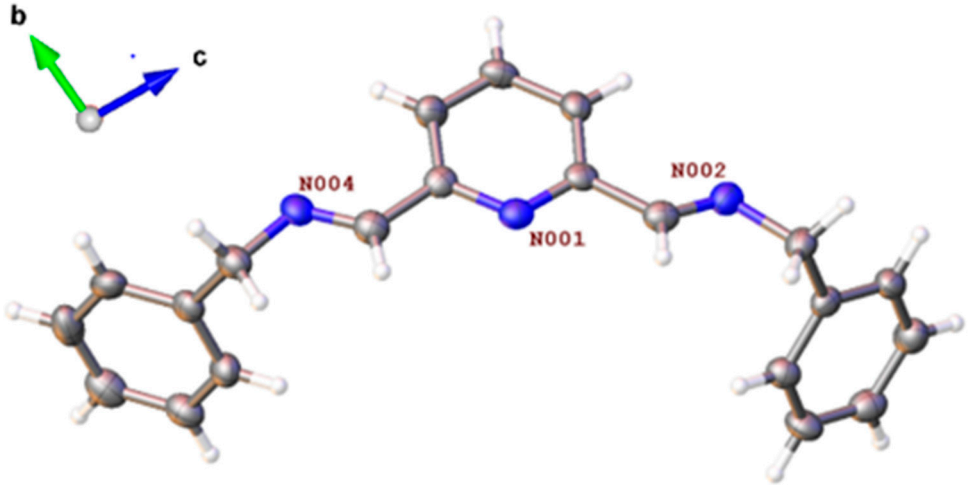

Figure 1. X-ray crystal structure of L^1 molecule in bc-axis; Color code: blue, N; grey, C; and white, H.

Table 3. Collated crystal parameters data for L^1, **1** and **2**.

Parameter	**L^1**	**1**	**2**
Empirical formula	$C_{21}H_{19}N_3$	$C_{43}H_{42}Cl_2FeN_6O_9$	$C_{46}H_{40}Cl_6FeN_8O_8$
Formula weight	313.39	912.44	1101.41
Temperature		120(2) K	
Wavelength		0.71073 Å	
Crystal system	Triclinic	Monoclinic	Triclinic
Space group	$P\bar{1}$	*C2/c*	$P\bar{1}$
Unit cell dimensions	a = 8.9002(19) Å b = 10.289(2) Å c = 19.181(4)Å α = 92.691(10)° β = 99.378(9)° γ = 100.078(10)°	a = 37.8848(9) Å b = 10.5130(3) Å c = 21.4945(5) Å α = 90° β = 109.7270(10)°γ = 90°	a = 10.1735(10) Å b = 10.2669(9) Å c = 23.149(2) Å α = 92.685(3)° β = 101.466(3)° γ = 90.261(3)°
Volume	1701.1(7) $Å^3$	8058.5(4) $Å^3$	2366.9(4) $Å^3$
Z	4	8	2
Calculated density	1.224 g/cm^3	1.509 g/cm^3	1.545 g/cm^3
Absorption coefficient	0.073 mm^{-1}	0.573 mm^{-1}	0.721 mm^{-1}
Crystal size	0.321 × 0.299 × 0.050 mm^3	0.248 × 0.220 × 0.104 mm^3	0.427 × 0.358 × 0.309 mm^3

Table 3. *Cont.*

Parameter	L^1	1	2
Theta range for data collection	2.016° to 26.570°	2.020° to 27.493°	2.043° to 27.573°
Limiting indices	$-11 \leq h \leq 10$; $-12 \leq k \leq 12$; $0 \leq l \leq 24$	$-48 \leq h \leq 49$; $-13 \leq k \leq 13$; $-23 \leq l \leq 27$	$-13 \leq h \leq 13$; $-12 \leq k \leq 13$; $-30 \leq l \leq 30$
Reflections collected/unique	7284/7284	54461/9242	71645/10877
Completeness to θ: fraction	25.242°: 100.0%	25.242°: 99.9%	25.242°: 99.7%
Absorption correction	Semi-empirical from equivalents		
Max. and min. transmission	1.00 and 0.65	0.95 and 0.87	0.91 and 0.77
Refinement method	Full-matrix least-squares on F^2		
Data/restraints/parameters	7284/0/434	9242/6/639	10877/25/683
Goodness-of-fit on F^2	1.020	1.047	1.144
Final R indices ($I > 2\sigma(I)$)	$R_1 = 0.0717$; $wR_2 = 0.1517$	$R_1 = 0.0354$; $wR_2 = 0.0779$	$R_1 = 0.1089$ $wR_2 = 0.2256$
R indices (all data)	$R_1 = 0.1317$; $wR_2 = 0.1819$	$R_1 = 0.0434$; $wR_2 = 0.0818$	$R_1 = 0.1308$; $wR_2 = 0.2359$
Largest diff. peak and hole	0.221 and -0.251×10^{-3} Å	0.572 and -0.463×10^{-3} Å	0.859 and -0.894×10^{-3} Å
Spin states	-	LS	LS
CCDC number	2165843	2154904	2128830

Table 4. Coordination bond lengths for **1** and **2** at 120 K.

Fe1–N Bond Lengths (Å) at 120 K			
1		**2**	
Fe(1)–N(2)	1.8794(14)	Fe(1)–N(2)	1.875(5)
Fe(1)–N(5)	1.8799(14)	Fe(1)–N(5)	1.880(5)
Fe(1)–N(3)	1.9763(15)	Fe(1)–N(4)	1.978(5)
Fe(1)–N(4)	1.9846(14)	Fe(1)–N(3)	1.981(5)
Fe(1)–N(6)	1.9891(16)	Fe(1)–N(6)	1.990(5)
Fe(1)–N(1)	1.9938(15)	Fe(1)–N(1)	1.998(5)
Average Fe1–N	1.9505(15)		1.950(5)

The single crystal X-ray diffraction data for the complexes **1** and **2** were collected at 120 K. Compound **1** crystallizes in a monoclinic crystal lattice with space group *C*2/*c*, whereas **2** crystalizes in a triclinic lattice with space group $P\bar{1}$. An asymmetric unit of **1** consists of one discrete $[FeL_2]^{2+}$ cation, two ClO_4^- ions and one methanol solvent molecule (Figure 2a). However, the asymmetric units of **2** contain one discrete $[FeL_2]^{2+}$ cation, two ClO_4^- ions and two acetonitrile solvent molecules (Figure 2b). The unit cell of **1** contains eight complex units, sixteen counter anions and eight solvent molecules, whereas **2** contains two complex units, four counter anions and four solvent molecules (Figure S2c,d).

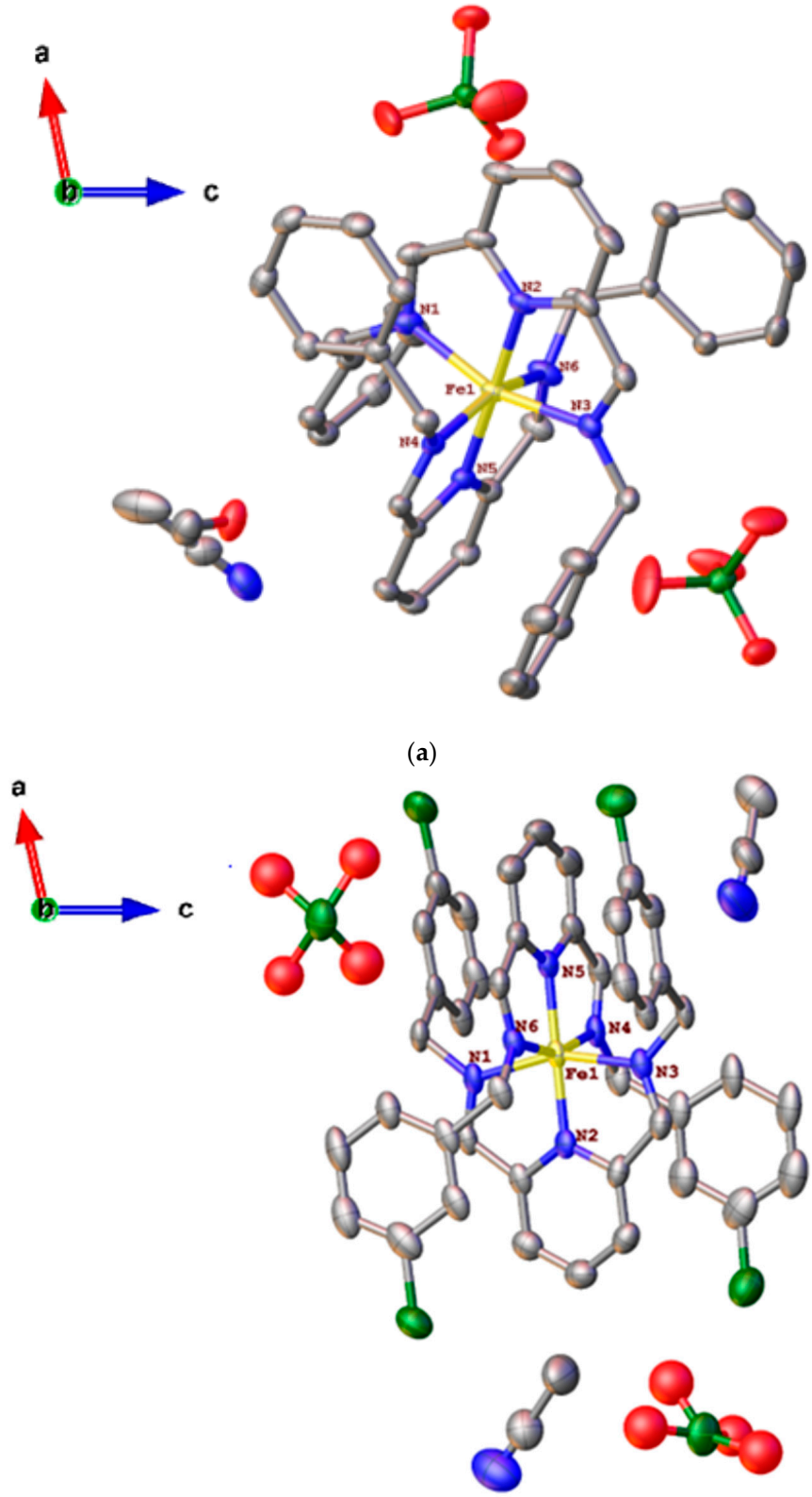

Figure 2. Labelled ORTEP drawing of **1** (**a**) and **2** (**b**) both in b-axis. Thermal ellipsoids are drawn on 30% probability level. Hydrogen atoms have been omitted for clarity. Color code: Yellow-green, Fe; blue, N; grey, C; green, Cl and red, O.

In both **1** and **2**, the coordination sphere is composed of six nitrogen donors. Two pyridine nitrogen atoms of both L^1 and L^2 occupy the axial positions and the four azomethine nitrogens occupy the equatorial plane (Scheme 1). Two tridentate ligands are wrapped around the Fe^{II} metal centers in a distorted octahedral geometry, with average Fe–N bond lengths of 1.9505 Å for **1** and 1.9643 Å for **2** (Table 4). These distances are indicative of LS Fe^{II} centers, which is in accordance with magnetic investigations, *vide infra* [39–41]. The average Fe–N_{py} and Fe–N_{imine} bond distances are 1.8797(14) Å and 1.9860(15) Å, respectively, for **1**, and 1.878(5) Å and 1.987(5) Å, respectively, for **2** (Table 4), which coincide very well with DFT optimized parameters for $[Fe(L^1)_2]^{2+}$ ($d(Fe–N_{py})_{avrgd}$ = 1.881 Å; $d(Fe–N_{imine})_{avrgd}$ = 1.983 Å) and $[Fe(L^2)_2]^{2+}$ ($d(Fe–N_{py})_{avrgd}$ = 1.884 Å; $d(Fe–N_{imine})_{avrgd}$ = 1.989 Å) in singlet (S = 0) states (see Supplementary Materials for TPSSh-D3(BJ)/def2-TZVP optimized geometries). The axial angles N(2)–Fe(1)–N(5) 178.92(6)° for **1** and 178.8(2)° for **2** indicate a clear distortion from the linear arrangement in both molecules (Table S3).

Hydrogen bonding and π-π stacking were found to have a marked influence on the magnetic properties of crystalline Fe^{II} complexes when they directly bridge individual ligands [42]. Upon inspection of the intermolecular interaction in the molecular packing of **1** and **2**, it was found that complex units form weak π-π interaction through phenyl rings in the ligands on the bc plane for **1** and ab plane for **2**, with an angle, centroid–centroid distances and shift distances of 3.140°, 3.715 and 1.810 Å, respectively, for **1**, and 2.321°, 3.840 and 1.676 Å, respectively, for **2** (Figure S2a,b). Moreover, hydrogen bonding occurs between the oxygen atom of perchlorate counteranion and hydrogen atom of methanol, ClO1···H9 with a distance of 1.969(13) Å for **1**, whereas for **2**, the disordered perchlorate counteranions interact via hydrogen bonding with the CH_2 group of the ligand moiety, O1E···H7A with a distance of 2.17(3) Å (Figure S2c,d). Hydrogen bonding interactions that are mediated by counteranions, as in our case, show negligible effects on the spin state of the metal center and are thereby locked in the LS state [43,44]. As regards the intermolecular interaction of **1**, the solvent CH_3OH forms short contacts with ClO_4^- ions with an average distance of 2.65(3) Å and the molecular packing of **2** shows that weak contact exists through the CH_2 group of the ligand moiety and ClO_4^- ion with an average distance of 2.58(2) Å [45] (Figure S2c,d).

2.3. Magnetic Studies

The temperature dependence of the molar magnetic susceptibility for **1** and **2** was measured with a SQUID magnetometer (MPMS XL, Quantum Design) in the DC mode at B_{DC} = 0.1 T. It was converted to the dimensionless product function. Its temperature dependence is shown in Figure 3a (**1**) and Figure 3b (**2**). Magnetic susceptibility measurements show that both complexes are completely locked in spin-paired diamagnetic states in the whole temperature range measured. This observation is in accordance with the average Fe–N bond observed—1.9505(15) Å for **1** and 1.950(5) Å for **2**—which is characteristic of Fe^{II} in a low spin state [20,27]. However, the very small positive susceptibility values observed in the temperature dependance of the molar susceptibility curves for **1** and **2** may be due to the temperature-independent paramagnetism. The diamagnetic nature of both Fe^{II} complexes is also supported in solution by characteristic, well-resolved ^1H and ^{13}C NMR peaks. These chemical shifts are in excellent accord with those computed at the TPSSh-D3(BJ)/def2-TZVP level for closed-shell (S = 0) species (see Tables S1 and S2 and Figure S1 in Supplementary Materials). High spin complexes in a quintet (S = 2) state are computed at the same level to be energetically disfavored by 76.0 kJ/mol and 72.9 kJ/mol for **1** and **2**, respectively. This relatively large energy gap can explain the locking of these complexes in the closed-shell state (S = 0) over a wide temperature range. A similar spin-paired, diamagnetic state has been observed for a N_6–coordination (two azomethine and one pyridyl nitrogen from each ligand) in $[FeL_2]^{2+}$ Schiff base complexes [35]. Our previous investigations revealed that the spin state cannot be changed by introducing an electron-donating methyl group to the ligand system mentioned above with N_6–coordination [34]. With the same type of hexa coordinate ligand systems, it has been observed that, if the

pyridyl nitrogen coordination is replaced by imidazole nitrogen, the compound exhibits SCO behavior [46]. It is worth noting that, with the similar type of coordination environment reported by Alberto et al. [47] and Ishida et al. [25], the HS state and SCO become stabilized by increasing the size of the halogen substituent. Moreover, Gu et al. have shown that the electron-donating methyl substitution, counteranion or solvent have a negligible influence on the SCO behavior [20,39], with the same type of N_6–ligand field, which is in accordance with the results that we have obtained.

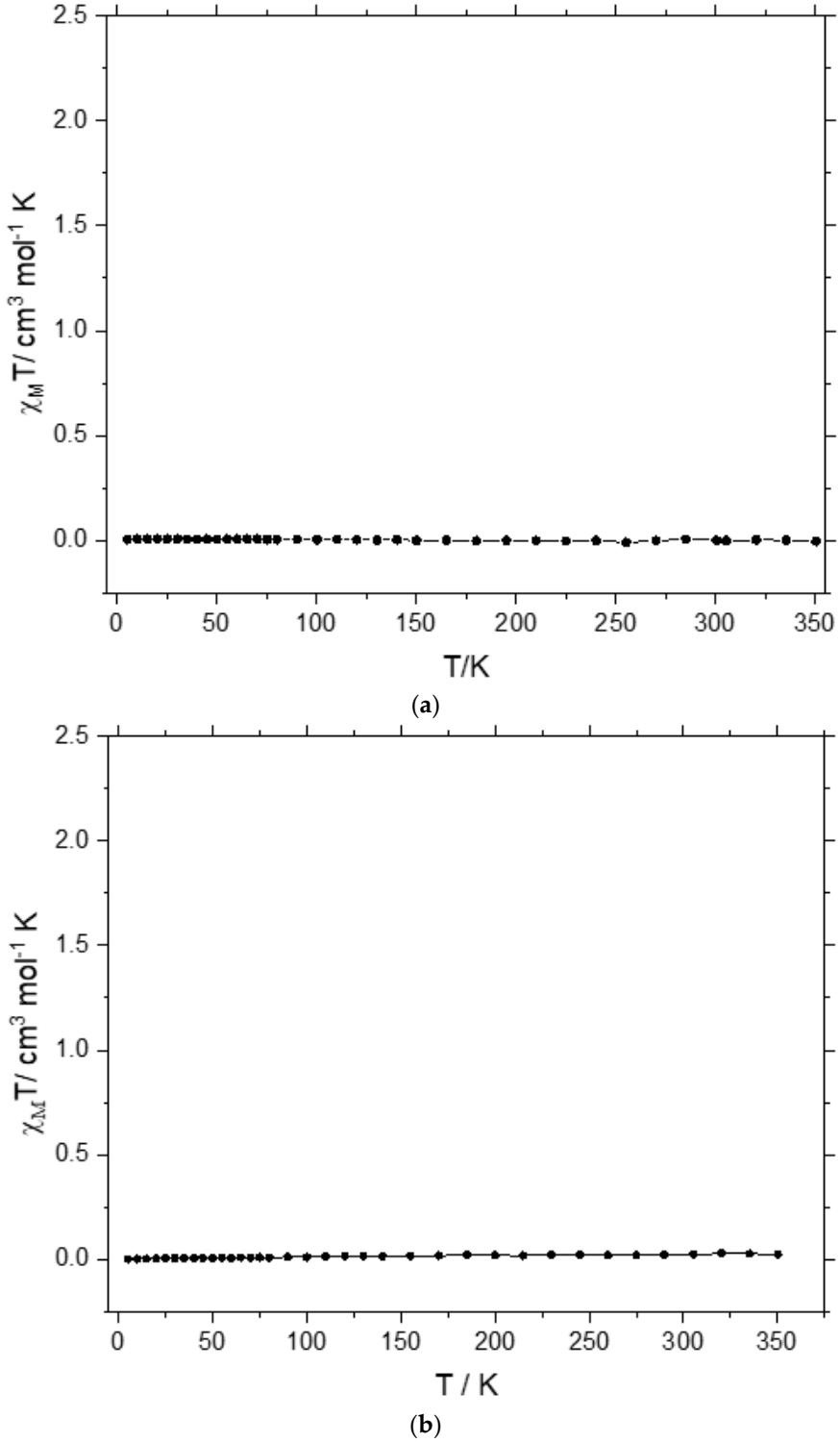

Figure 3. The $\chi_M T$ vs. T magnetic plots for **1** (**a**) and **2** (**b**) between 5–350 K.

3. Materials and Methods

All chemicals and reagents were purchased from commercial sources and were of analytical reagent grade, used without further purification. All complexation reactions were carried out under nitrogen atmosphere. FTIR spectra were measured on an Agilent Technologies Cary 630 FTIR spectrometer in the 4000–400 cm^{-1} range. NMR spectra were recorded with Bruker Ascend^{TM} (Billerica, MA, USA) 400 (400 MHz for ^{1}H and 101 MHz for ^{13}C) instruments in CD_3CN with tetramethylsilane (TMS) as an internal reference. Elemental analyses were carried out on a FLASH elemental analyzer 1112 CHNS-O (Thermo Finnigan Italia, Rodano, Italy). Melting points were determined on a Büchi Melting Point M-565 apparatus. Single crystal XRD measurements were performed with a Bruker D8 VENTURE Kappa Duo diffractometer equipped with a PHOTON III detector and using monochromatic CuK_α primary radiation. The phase problem was solved by intrinsic phasing (SHELXT) [48] and the structure model was refined by full-matrix least-squares on F^2 values (SHELXL) [49]. Magnetic susceptibility measurements were carried out on a SQUID magnetometer (Quantum Design MPMS XL, San Diego, CA, USA) operating between 5 and 350 K with magnetic fields 1 kOe. The data were corrected for the intrinsic diamagnetic contributions of the sample and the sample holder. Electrospray ionization–mass spectrometry was performed using ESI-ToF Mass spectrometer (Bruker Daltonics micrOTOF-Q II).

CAUTION. Handling with metal–organic perchlorates is potentially dangerous due to their explosive properties. It should be handled with care in small quantities. Especially high temperature magnetic measurements are risky.

3.1. Synthesis

3.1.1. Synthesis of the Schiff Bases L^1 and L^2

The tridentate Schiff base ligands L^1 ((*E*,*E*)-2,6-bis[(benzylimino)methyl)pyridine) were prepared by modified literature procedures [50,51], where a solution of benzylamine (0.65 mL, 6 mmol) and L^2 ((*E*,*E*)-2,6-bis[(3-chlorobenzylimino)methyl]pyridine) 3-chlorobenzylamine (0.90 mL, 6 mmol) in ethanol (15 mL) were mixed with a stirred solution of pyridine-2,6-dicarbaldehyde (0.41 g, 3 mmol) in hot ethanol (15 mL). The mixtures were refluxed for 4 h (Scheme 1), while no precipitation occurred. The resultant solutions were concentrated to 10 mL and agitated thoroughly with a small amount of petroleum ether at 70–80 °C, which led to the precipitation of the ligands. These were then filtered, washed with petroleum ether and dried in vacuum. Pale orange (L^1) and off-white (L^2) needle-like crystalline products were collected.

L^1: Yield; 85%; M. P. 75 °C; Anal. $C_{21}H_{19}N_3$: Calcd. C 80.51, H 6.07, N 13.42; found C 80.46, H 6.08, N 13.51%; ^{1}H NMR (CD_3CN): δ(ppm) = 8.42 (s, 2H, CH-azomethine), 7.97 (d, *J* = 7.8 Hz, 2H, pyridine), 7.79 (t, *J* = 7.8 Hz, 1H, pyridine), 7.30 (m, 4H, Ar), 7.29 (m, 4H, Ar), 7.21 (m, 2H, Ar) and 4.89 (s, 4H, 2 × CH_2). ^{13}C NMR (CD_3CN): δ(ppm) = 162.35 (C=N, azomethine), 154.55 (C-N, pyridine), 139.32, 137.49, 128.51, 128.19, 127.05, 121.83, 64.31 (Figure S3a,b). IR: $\overline{\nu}$ (cm^{-1}) = 3055(w), 3026(w), 2839(w), 1644(s), 1570(s), 1493(m), 1450(s), 1354(w), 1154(m), 1073(m), 1027(s), 991(m), 806(m) and 730(s).

L^2: Yield; 47.3%; M. P. 74.3 °C; Anal. $C_{21}H_{17}N_3Cl_2$: Calcd. C 65.96, H 4.45, N 10.99; found C 65.80, H 4.61 N 10.87%; M. Pt. 63.4; ^{1}H NMR (CD_3CN): δ(ppm) = 8.43 (s, 2H, azomethine), 8.00 (d, *J* = 7.8 Hz, 2H, pyridine), 7.81 (t, *J* = 7.8 Hz, 1H, pyridine), 7.34 (bs, 2H, Ar), 7.29–7.20 (m, 6H, Ar) and 4.77 (s, 4H, 2 × CH_2). ^{13}C NMR (CD_3CN): δ(ppm) = 162.99 (C=N, azomethine), 154.43 (C-N, pyridine), 141.83, 137.56, 133.77, 130.13, 127.97, 127.00, 126.56, 122.03, 63.41 (Figure S4a,b). IR: $\overline{\nu}$ (cm^{-1}) = 3060(w), 3026(w), 2839(w), 1651(s), 1594(s), 1571(s), 1472(s), 1429(s), 1335(w), 1200(m), 1157(m), 1074(s), 995(m), 864(m) and 744(s).

3.1.2. Synthesis of the Complex $[Fe(L^1)_2](ClO_4)_2 \cdot CH_3OH$ (**1**)

To a stirred solution of L^1 (0.313 g, 1.0 mmol) in methanol (20 mL), $Fe(ClO_4)_2 \cdot 6H_2O$ (0.181 g, 0.5 mmol) was added under nitrogen atmosphere. The resultant purple solution was refluxed for 2 h under continuous stirring (Scheme 1). It was then cooled and filtered.

Slow diffusion of diethyl ether vapor into the filtered solution for two weeks afforded block-shaped black crystals suitable for X-ray diffraction measurements. The crystals were then filtered and washed with cold methanol and dried subsequently under vacuum overnight. Yield: 0.266 g, 58.3%; Anal. $C_{43}H_{42}Cl_2FeN_6O_9$, Calcd.: C 56.55; H 4.60; N 9.21; Found: C 56.77; H 4.78; N 9.16%. ^{1}H NMR(CD_3CN): δ(ppm) = 8.38 (t, *J* = 7.9 Hz, 2H, pyridine), 8.13 (d, *J* = 7.9 Hz, 4H, pyridine), 7.73 (s, 4H, azomethine), 7.29 (t, *J* = 7.4 Hz, 4H, Ar), 7.16 (t, *J* = 7.7 Hz, 8H, Ar), 6.47 (d, *J* = 7.6 Hz, 8H, Ar) and 3.68 (s, 8H, 4 × CH_2). ^{13}C NMR(CD_3CN): δ(ppm) = 170.05, 160.27, 137.43, 133.27, 129.34, 129.28, 128.70, 128.46 and 62.39 (Figure S5a,b). FTIR: (cm^{-1}) = 3021(w),1603(s), 1585(m), 1528(s), 1485(s), 1382(s), 1208(m), 1159(m), 1072(s), 980(m), 821(m), 740(s), 688(s), 620(s) and 450(s). ESI-MS: 781.20 (M^+-ClO_4^-), and 681.24 (M^{2+}) (Figure S7a).

3.1.3. Synthesis of the Complex $[Fe(L^2)_2](ClO_4)_2 \cdot 2CH_3CN$ (**2**)

The ligand L^2 (0.191 g, 0.5 mmol) was dissolved in acetonitrile (20 mL) and this solution was mixed with $Fe(ClO_4)_2 \cdot 6H_2O$ (0.090 g, 0.25 mmol) under nitrogen atmosphere. The resultant purple solution was refluxed for 2 h under continuous stirring (Scheme 1). The reaction mixture was then cooled and filtered. Slow diffusion of diethyl ether into the filtered solution yielded blocks of black crystals appropriate for X-ray diffraction. These were then filtered off, washed with cold acetonitrile and subsequently dried under vacuum. Yield: 0.213 g, 77.2%; Anal. $C_{46}H_{40}Cl_6FeN_8O_8$, Calcd.: C, 50.12; H, 3.63; N, 10.17; Found: C, 49.98; H, 3.74; N, 10.18%. ^{1}H NMR(CD_3CN): δ(ppm) = 8.50 (t, *J* = 7.9 Hz, 2H, pyridine), 8.23 (d, *J* = 7.9 Hz, 4H, pyridine), 7.84 (s, 4H, azomethine), 7.33 (d, *J* = 9.5 Hz, 4H, Ar), 7.17 (t, *J* = 9.5 Hz, 4H, Ar), 6.48 (bs, 8H, Ar) and 3.74 (s, 8H, 4 × CH_2). ^{13}C NMR(CD_3CN): δ(ppm) = 171.14, 160.36, 137.75, 135.49, 134.50, 130.94, 129.61, 128.74, 128.62, 127.26 and 61.79 (Figure S6a,b). FTIR: $\overline{\nu}$ (cm^{-1}) = 3044(w), 1600(s), 1564(s), 1529(s), 1474(s), 1396(s), 1355(m), 1194(m), 1075(s), 928(m), 852(m), 789(s), 705(s), 678(s), 614(s) and 442(s). ESI-MS: 917.04 (M^+–ClO_4^-) and 818.09 (M^{2+}) (Figure S7b).

3.2. Computational Details

The structures of all systems under investigation were fully optimized (without counteranion) in Turbomole [52] at the TPSSh level of theory, [53] including an atom-pairwise correction for dispersion forces (Grimme's D3 model) with Becke–Johnson (BJ) damping [54,55] and employing the def2-TZVP basis set for all atoms [56]. The optimized structures were characterized as true minima on the potential energy hypersurface by harmonic vibrational frequency analyses. Calculations of NMR nuclear shieldings were performed in the Gaussian 16 program package [57] using gauge-including atomic orbitals (GIAO) at the same level as structure optimization (TPSSh-D3(BJ)/def2-TZVP). In these calculations, bulk solvent effects were simulated by means of the integral equation formalism of the polarizable continuum model (IEF-PCM) [58]. The calculated ^{1}H and ^{13}C shieldings were converted to chemical shifts (δ in ppm) relative to the shieldings of tetramethylsilane (TMS).

4. Conclusions

Two mononuclear Fe^{II} complexes, $[Fe(L^1)_2](ClO_4)_2 \cdot CH_3OH$ (**1**) and $[Fe(L^1)_2](ClO_4)_2 \cdot 2CH_3CN$ (**2**), based on two unsymmetrical tridentate Schiff base ligands, were synthesized and characterized. Both complexes show distorted octahedral coordination geometries. Spectroscopic, magnetic and structural studies revealed that the spin states of both complexes remain diamagnetic throughout the measured temperature range. The ligand field created by N_6-coordination was comprised of four azomethine and two pyridine nitrogen favors, thus showing a low spin Fe^{II} state. It is notable that the variation of solvents (acetonitrile and/or methanol) did not influence the magnetic properties of **1** and **2**. Introducing an electron-withdrawing chlorine substituent into the meta position of L^2 did not alter the ligand field, and hence, there is no change in the spin state. We hope the observed results are of particular importance for further design of molecular magnetic materials and

encourage the development of new Fe^{II} Schiff base SCO systems. Further investigations by varying the ligand field and making substitutions in the ligand moiety are under way.

Supplementary Materials: The following supporting information can be downloaded at: https://www.mdpi.com/article/10.3390/inorganics10070098/s1, Figure S1: Comparison of calculated and experimental NMR shifts in [FeL2]2+ (S = 0) complexes (cf. Tables S1 and S2 for numeric data); Figure S2: Projection of the π-π interaction through phenyl rings of 1 (a) along the bc plane and 2 (b) along the ab plane. ClO4-ions, solvents and hydrogen atoms have been omitted for clarity. Short intermolecular contacts and H-bonding 1 (c) and 2 (d) both in b-direction; Figure S3: (a) 1H NMR and (b) 13C NMR of L1; Figure S4: (a) 1H NMR and (b) 13C NMR of L2; Figure S5: (a) 1H NMR and (b) 13C NMR of 1; Figure S6: (a) 1H NMR and (b) 13C NMR of 2; Figure S7: ESI-MS molecular ion peaks of 1 (a) and 2 (b); Table S1: Experimental and computed 1H NMR shifts (in ppm vs. TMS) in free ligands L1, L2 and corresponding [Fe(L1)2]2+ and [Fe(L2)2]2+ complexes (all in CD3CN); Table S2: Experimental and computed 13C NMR shifts (in ppm vs. TMS) in free ligands L1, L2 and corresponding [Fe(L1)2]2+ and [Fe(L2)2]2+ complexes (all in CD3CN); Table S3: Coordination bond angles for **1** and **2** at 120 K.

Author Contributions: The major work for this article, designing, execution and writing of the original draft, was done by the first author (Y.B.), which is part of his Ph.D. program. The second and third authors, N.S. and S.S. have done SQUID and ESI-MS measurements. The fourth author, R.G. solved the structures. The other authors, W.L., M.R., A.S., P.H. and M.T. were responsible for supervision, editing, and reviewing of this article. All authors have read and agreed to the published version of the manuscript.

Funding: This research project was supported by the National Scholarship Programme of the Slovak Republic 2021 and Addis Ababa Science and Technology University, Addis Ababa, Ethiopia. This work was also supported by the Slovak Research and Development Agency (Grant No. APVV-17-0324) and the Grant Agency of the Ministry of Education of the Slovak Republic (VEGA Project No. 1/0669/22).

Institutional Review Board Statement: Not applicable.

Informed Consent Statement: Not applicable.

Data Availability Statement: Not applicable.

Acknowledgments: We are thankful to National Scholarship Programme of the Slovak Republic 2021 for a research stay and Woldia University, Ethiopia, for a Ph.D studentship to Y.B. Thanks are due to Patrik Osuský, Department of Inorganic Chemistry, Comenius University, Slovakia, for spectroscopic measurements. We are also grateful to Jozef Noga, Department of Inorganic Chemistry, Comenius University, Slovakia, for his keen interest and support during this work.

Conflicts of Interest: The authors declare no conflict of interest.

References

1. Cambi, L.; Szego, L. The Magnetic Susceptibility of Complex Compounds. *Ber. Dtsch. Chem. Ges* **1931**, *64*, 2591–2598. [CrossRef]
2. Gutlich, P.; Goodwin, H. Spin Crossover in Transition Metal Compounds I–III. In *Topics in Current Chemistry*; Springer: New York, NY, USA; Berlin/Heidelberg, Germany, 2004; pp. 2–356, ISBN 3540403949.
3. Miller, J.S.; Gatteschi, D. Molecule-Based Magnets Themed Issue. *Chem. Soc. Rev.* **2011**, *40*, 3313–3335. [CrossRef]
4. Senthil Kumar, K.; Ruben, M. Emerging Trends in Spin Crossover (SCO) Based Functional Materials and Devices. *Coord. Chem. Rev.* **2017**, *346*, 176–205. [CrossRef]
5. Sugimoto, K.; Okubo, T.; Maekawa, M.; Kuroda-Sowa, T. Visualization of Weak Interaction Effects on N_2O Schiff Base Ligands in Iron(II) Spin Crossover Complexes. *Cryst. Growth Des.* **2021**, *21*, 4178–4183. [CrossRef]
6. Aromi, G.; Real, J.A. Special Issue "Spin Crossover (SCO) Research". *Magnetochemistry* **2016**, *2*, 2–4. [CrossRef]
7. Swart, M.; Costas, M. *Spin States in Biochemistry and Inorganic Chemistry Influence on Structure and Reactivity*, 1st ed.; Swart, M.C., Ed.; John Wiley & Sons, Ltd.: Chichester, UK, 2016; ISBN 9781118898314.
8. Senthil Kumar, K.; Bayeh, Y.; Gebretsadik, T.; Elemo, F.; Gebrezgiabher, M.; Thomas, M.; Ruben, M. Spin Crossover in Iron(II) Schiff Base Complexes. *Dalton Trans.* **2019**, *48*, 15321–15337. [CrossRef]
9. Zhong, Z.J.; Tao, J.Q.; Zhi, Y.; Dun, C.Y.; Liu, Y.J.; You, X.Z. A Stacking Spin Crossover Iron(II) Compound with a Large Hysteresis. *J. Chem. Soc. Dalton Trans.* **1998**, *2*, 327–328. [CrossRef]

10. Real, J.A.; Gaspar, A.B.; Carmen Muñoz, M. Thermal, Pressure and Light Switchable Spin Crossover Materials. *Dalton Trans.* **2005**, *12*, 2062–2079. [CrossRef]
11. Halcrow, M.A. *Spin-Crossover Materials Properties and Applications*; John Wiley & Sons, Ltd.: Chichester, UK, 2013.
12. Antonio, J.; Ana, R.; Carmen, B.G.M.; Gütlich, P.; Ksenofontov, V.; Spiering, H.; Chemie, A. Bipyrimidine-Bridged Dinuclear Iron(II) Spin Crossover Compounds. *Top. Curr. Chem.* **2004**, *233*, 167–193. [CrossRef]
13. Brooker, S. Spin Crossover with Thermal Hysteresis: Practicalities and Lessons Learnt. *Chem. Soc. Rev.* **2015**, *44*, 2880–2892. [CrossRef]
14. Halcrow, M.A. Structure: Function Relationships in Molecular Spin Crossover Complexes W. *Chem. Soc. Rev.* **2011**, *40*, 4119–4142. [CrossRef] [PubMed]
15. Gamez, P.; Costa, J.S.; Quesada, M.; Aromi, G. Iron Spin Crossover Compounds: From Fundamental Studies to Practical Applications. *Dalton Trans.* **2009**, *38*, 7845–7853. [CrossRef] [PubMed]
16. Murray, K.S.; Kepert, C.J. Cooperativity in Spin Crossover Systems: Memory, Magnetism and Microporosity. *Top. Curr. Chem.* **2006**, *233*, 195–228. [CrossRef]
17. Weber, B.; Bauer, W.; Obel, J. An Iron (II) Spin Crossover Complex with a 70 K Wide Thermal. *Angew. Chem. Int. Ed.* **2008**, *47*, 10098–10101. [CrossRef] [PubMed]
18. Gaspar, A.B.; Mun, M.C. Dinuclear Iron (II) Spin Crossover Compounds: Singular Molecular Materials for Electronics. *J. Mater. Chem.* **2006**, *16*, 2522–2533. [CrossRef]
19. Schäfer, B.; Bauer, T.; Faus, I.; Wolny, J.A.; Dahms, F.; Fuhr, O.; Lebedkin, S.; Wille, H.C.; Schlage, K.; Chevalier, K.; et al. A Luminescent Pt2Fe Spin Crossover Complex. *Dalton Trans.* **2017**, *46*, 2289–2302. [CrossRef] [PubMed]
20. Wang, Y.T.; Li, S.T.; Wu, S.Q.; Cui, A.L.; Shen, D.Z.; Kou, H.Z. Spin Transitions in Fe(II) Metallogrids Modulated by Substituents, Counteranions, and Solvents. *J. Am. Chem. Soc.* **2013**, *135*, 5942–5945. [CrossRef] [PubMed]
21. Weber, B. Spin Crossover Complexes with N_4O_2 Coordination Sphere-The Influence of Covalent Linkers on Cooperative Interactions. *Coord. Chem. Rev.* **2009**, *253*, 2432–2449. [CrossRef]
22. Halcrow, M.A. Spin-Crossover Compounds with Wide Thermal Hysteresis. *Chem. Lett.* **2014**, *43*, 178–1188. [CrossRef]
23. Lochenie, C.; Bauer, W.; Railliet, A.P.; Schlamp, S.; Garcia, Y.; Weber, B. Large Thermal Hysteresis for Iron(II) Spin Crossover Complexes with N-(Pyrid-4-Yl)Isonicotinamide. *Inorg. Chem.* **2014**, *53*, 11563–11572. [CrossRef]
24. Phonsri, W.; Macedo, D.S.; Vignesh, K.R.; Rajaraman, G.; Davies, C.G.; Jameson, G.N.L.; Moubaraki, B.; Ward, J.S.; Kruger, P.E.; Chastanet, G.; et al. Halogen Substitution Effects on N2O Schiff Base Ligands in Unprecedented Abrupt Fe(II) Spin Crossover Complexes. *Chem. Eur. J.* **2017**, *23*, 7052–7065. [CrossRef] [PubMed]
25. Kimura, A.; Ishida, T. Spin Crossover Temperature Predictable from DFT Calculation for Iron(II) Complexes with 4-Substituted Pybox and Related Heteroaromatic Ligands. *ACS Omega* **2018**, *3*, 6737–6747. [CrossRef]
26. Mochida, N.; Kimura, A.; Ishida, T. Spin Crossover Hysteresis of [FeII (LHiPr)2(NCS)2](LHiPr = N-2-Pyridylmethylene-4 Isopropylaniline) Accompanied by Isopropyl Conformation Isomerism. *Magnetochemistry* **2015**, *1*, 17–27. [CrossRef]
27. Halcrow, M.A. The Spin-States and Spin Transitions of Mononuclear Iron(II) Complexes of Nitrogen-Donor Ligands. *Polyhedron* **2007**, *26*, 3523–3576. [CrossRef]
28. Kershaw Cook, L.J.; Kulmaczewski, R.; Mohammed, R.; Dudley, S.; Barrett, S.A.; Little, M.A.; Deeth, R.J.; Halcrow, M.A. A Unified Treatment of the Relationship between Ligand Substituents and Spin State in a Family of Iron (II) Complexes. *Angew. Chem. Int. Ed.* **2016**, *55*, 4327–4331. [CrossRef]
29. Létard, J.F.; Guionneau, P.; Nguyen, O.; Costa, J.S.; Marcén, S.; Chastanet, G.; Marchivie, M.; Goux-Capes, L. A Guideline to the Design of Molecular-Based Materials with Long-Lived Photomagnetic Lifetimes. *Chem. Eur. J.* **2005**, *11*, 4582–4589. [CrossRef] [PubMed]
30. Yamasaki, M.; Ishida, T. Heating-Rate Dependence of Spin Crossover Hysteresis Observed in an Iron(II) Complex Having Tris (2-Pyridyl)Methanol. *J. Mater. Chem. C* **2015**, *3*, 7784–7787. [CrossRef]
31. Phonsri, W.; Harding, D.J.; Harding, P.; Murray, K.S.; Moubaraki, B.; Gass, I.A.; Cashion, J.D.; Jameson, G.N.L.; Adams, H. Stepped Spin Crossover in Fe(III) Halogen Substituted Quinolylsalicylaldimine Complexes. *Dalton Trans.* **2014**, *43*, 17509–17518. [CrossRef]
32. Madhu, N.T.; Salitros, I.; Schramm, F.; Klyatskaya, S.; Fuhr, O.; Ruben, M. Above Room Temperature Spin Transition in a Series of Iron(II) Bis(Pyrazolyl)Pyridine Compounds. *C. R. Chim.* **2008**, *11*, 1166–1174. [CrossRef]
33. Salitros, I.; Madhu, N.T.; Boca, R.; Pavlik, J.; Ruben, M. Room-Temperature Spin-Transition Iron Compounds. *Monatsh. Chem.* **2009**, *140*, 695–733. [CrossRef]
34. Bayeh, Y.; Osusky, P.; Gyepes, R.; Yutronkie, N.J.; Sergawie, A.; Hrobarik, P.; Clerac, R.; Madhu, T. Low-Spin Mononuclear Iron(II) Complexes Based on Tridentate N-Donor Schiff Base Ligand Derived from Pyridine-2,6-dicarboxaldehyde. *Polyhedron* 2022, *under preparation*.
35. Stratton, W.J.; Busch, D.H. The Complexes of Pyridinaldazine with Iron(II) and Nickel(II). *J. Am. Chem. Soc.* **1958**, *80*, 1286–1289. [CrossRef]
36. Nakamoto, K. *Infrared and Raman Spectra of Inorganic and Coordination Compounds Part B: Theory and Applications*; John Wiley & Sons, Inc.: Hoboken, NJ, USA, 1978; Volume 156, ISBN 9780471744931.
37. Nakamoto, K. *Infrared and Raman Spectra of Inorganic and Coordination Compounds: Part A: Theory and Applications in Inorganic Chemistry*, 6th ed.; John Wiley & Sons, Inc.: Hoboken, NJ, USA, 2008.

38. Hagiwara, H.; Tanaka, T.; Hora, S. Synthesis, Structure, and Spin Crossover above Room Temperature of a Mononuclear and Related Dinuclear Double Helicate Iron(II) Complexes. *Dalton Trans.* **2016**, *45*, 17132–17140. [CrossRef] [PubMed]
39. Han, W.K.; Li, Z.H.; Zhu, W.; Li, T.; Li, Z.; Ren, X.; Gu, Z.G. Molecular Isomerism Induced Fe(II) Spin State Difference Based on the Tautomerization of the 4(5)-Methylimidazole Group. *Dalton Trans.* **2017**, *46*, 4218–4224. [CrossRef] [PubMed]
40. Milin, E.; Benaicha, B.; El Hajj, F.; Patinec, V.; Triki, S.; Marchivie, M.; Gómez-García, C.J.; Pillet, S. Magnetic Bistability in Macrocycle-Based Fe(II) Spin Crossover Complexes: Counter Ion and Solvent Effects. *Eur. J. Inorg. Chem.* **2016**, *2016*, 5282. [CrossRef]
41. Marchivie, M.; Guionneau, P.; Létard, J.F.; Chasseau, D. Photo-Induced Spin-Transition: The Role of the Iron(II) Environment Distortion. *Acta Crystallogr. Sect. B Struct. Sci.* **2005**, *61*, 25–28. [CrossRef]
42. Létard, J.F.; Guionneau, P.; Rabardel, L.; Howard, J.A.K.; Goeta, A.E.; Chasseau, D.; Kahn, O. Structural, Magnetic, and Photomagnetic Studies of a Mononuclear Iron(II) Derivative Exhibiting an Exceptionally Abrupt Spin Transition. Light-Induced Thermal Hysteresis Phenomenon. *Inorg. Chem.* **1998**, *37*, 4432–4441. [CrossRef]
43. Ikuta, Y.; Ooidemizu, M.; Yamahata, Y.; Yamada, M.; Osa, S.; Matsumoto, N.; Iijima, S.; Sunatsuki, Y.; Kojima, M.; Dahan, F.; et al. A New Family of Spin Crossover Complexes with a Tripod Ligand Containing Three Imidazoles. *Inorg. Chem.* **2003**, *42*, 7001–7017. [CrossRef]
44. Matouzenko, G.S.; Molnar, G.; Bréfuel, N.; Perrin, M.; Bousseksou, A.; Borshch, S.A. Spin Crossover Iron(II) Coordination Polymer with Zigzag Chain Structure. *Chem. Mater.* **2003**, *15*, 550–556. [CrossRef]
45. Buron-Le Cointe, M.; Hébert, J.; Baldé, C.; Moisan, N.; Toupet, L.; Guionneau, P.; Létard, J.F.; Freysz, E.; Cailleau, H.; Collet, E. Intermolecular Control of Thermoswitching and Photoswitching Phenomena in Two Spin-Crossover Polymorphs. *Phys. Rev. B* **2012**, *85*, 39–41. [CrossRef]
46. Craze, A.R.; Howard-Smith, K.J.; Bhadbhade, M.M.; Mustonen, O.; Kepert, C.J.; Marjo, C.E.; Li, F. Investigation of the High-Temperature Spin-Transition of a Mononuclear Iron(II) Complex Using X-Ray Photoelectron Spectroscopy. *Inorg. Chem.* **2018**, *57*, 6503–6510. [CrossRef]
47. Rodríguez-Velamazán, J.A.; Carbonera, C.; Castro, M.; Palacios, E.; Kitazawa, T.; Létard, J.F.; Burriel, R. Two-Step Thermal Spin Transition and LIESST Relaxation of the Polymeric Spin Crossover Compounds $Fe(X\text{-}Py)_2[Ag(CN)_2]_2$ (X = H, 3-Methyl, 4-Methyl, 3,4-Dimethyl, 3-Cl). *Chem. Eur. J.* **2010**, *16*, 8785–8796. [CrossRef] [PubMed]
48. Sheldrick, G.M. SHELXT—Integrated Space-Group and Crystal-Structure Determination. *Acta Crystallogr. Sect. A Found. Crystallogr.* **2015**, *71*, 3–8. [CrossRef] [PubMed]
49. Sheldrick, G.M. Crystal Structure Refinement with SHELXL. *Acta Crystallogr. Sect. C Struct. Chem.* **2015**, *71*, 3–8. [CrossRef] [PubMed]
50. Lewkowski, J.; Dzięgielewski, M. Stereochemistry of Phosphite Addition to Azomethine Bond of Achiral 2,6-Pyridinedicarbaldimines and Isophthalaldimines—A Comparative Study. *Phosphorus Sulfur Silicon Relat. Elem.* **2013**, *188*, 995–1006. [CrossRef]
51. Scrimin, P.; Tecilla, P.; Tonellato, U.; Valle, G.; Veronese, A. Metal Ions Co-Operativity in the Catalysis of the Hydrolysis of a β-Amino Ester by a Macrocyclic Dinuclear Cu (II) Complex. *Tetrahedron* **1995**, *51*, 527–538. [CrossRef]
52. *TURBOMOLE*, Version 7.5; TURBOMOLE GmbH, a Development of the University of Karlsruhe and Forschungszentrum Karlsruhe. 2020. Available online: http://www.turbomole.com (accessed on 29 May 2022).
53. Tao, J.; Perdew, J.P.; Staroverov, V.N.; Scuseria, G.E. Climbing the Density Functional Ladder: Nonempirical Meta–Generalized Gradient Approximation Designed for Molecules and Solids. *Phys. Rev. Lett.* **2003**, *91*, 3–6. [CrossRef]
54. Grimme, S.; Antony, J.; Ehrlich, S.; Krieg, H. A Consistent and Accurate Ab Initio Parametrization of Density Functional Dispersion Correction (DFT-D) for the 94 Elements H-Pu. *J. Chem. Phys.* **2010**, *132*, 154104. [CrossRef]
55. Grimme, S.; Ehrlich, S.; Goerigk, L. Effect of the Damping Function in Dispersion Corrected Density Functional Theory. *J. Comput. Chem.* **2011**, *32*, 1456–1465. [CrossRef]
56. Weigend, F.; Ahlrichs, R. Balanced Basis Sets of Split Valence, Triple Zeta Valence and Quadruple Zeta Valence Quality for H to Rn: Design and Assessment of Accuracy. *Phys. Chem. Chem. Phys.* **2005**, *7*, 3297–3305. [CrossRef]
57. Frisch, M.J.; Trucks, G.W.; Schlegel, H.B.; Scuseria, G.E.; Robb, M.A.; Cheeseman, J.R.; Scalmani, G.; Barone, V.; Petersson, G.A.; Petersson, H.; et al. *Gaussian 16*; revision C.01; Gaussian, Inc.: Wallingford, UK, 2016.
58. Tomasi, J.; Mennucci, B.; Cammi, R. Quantum Mechanical Continuum Solvation Models. *Chem. Rev.* **2005**, *105*, 2999–3093. [CrossRef]